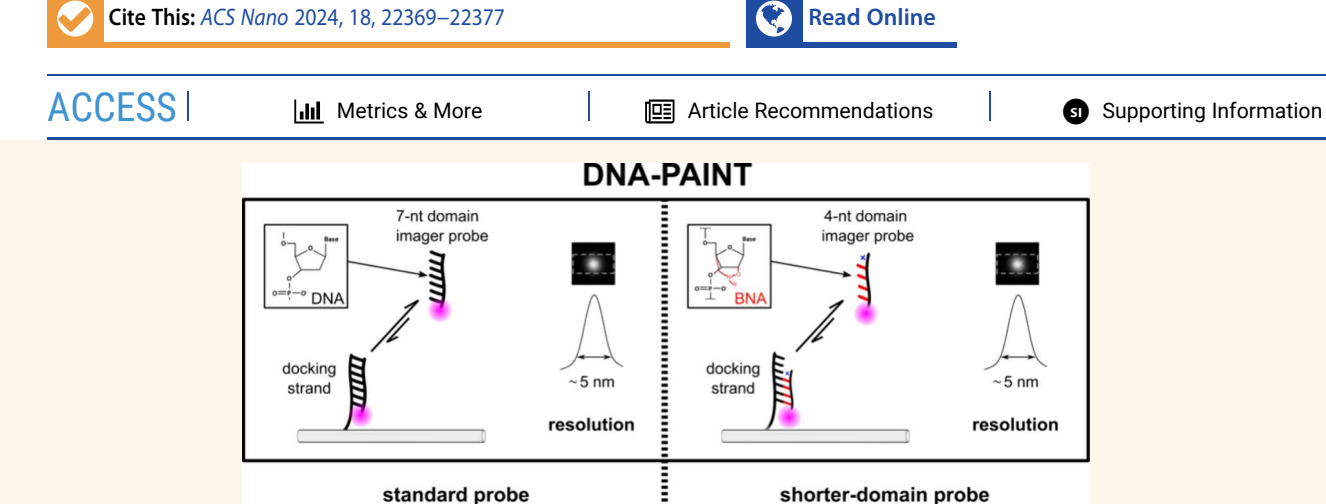
www.acsnano.org

See https://pubs.acs.org/sharingguidelines for options on how to legitimately share published articles

Downloaded via CORNELL UNIV on October 1, 2024 at 02:17:56 (UTC).

DNA-PAINT Probe Modifications Support High-Resolution Imaging with Shorter Binding Domains

Luca Piantanida, George D. Dickinson, Jacob M. Majikes, William Clay, J. Alexander Liddle, Tim Andersen, Eric J. Hayden, Wan Kuang, and William L. Hughes*



ABSTRACT: DNA-based Points Accumulation for Imaging in Nanoscale Topography (DNA-PAINT) is an effective super resolution microscopy technique, and its optimization is key to improve nanoscale detection. The state-of-theart improvements that are at the base of this optimization have been first routinely validated on DNA nanostructure devices before being tested on biological samples. This allows researchers to finely tune DNA-PAINT imaging features in a more controllable in vitro environment. Dye-labeled oligonucleotide probes with short hybridization domains can expand DNA-PAINT's detection by targeting short nucleotide sequences and improving resolution, speed, and multiplexing. However, developing these probes is challenging as their brief bound state makes them difficult to capture under routine imaging conditions. To extend dwell binding times and promote duplex stability, we introduced structural and chemical modifications to our imager probes. The modifications included minihairpins and/or Bridged Nucleic Acids (BNA); both of which increase the thermomechanical stability of a DNA duplex. Using this approach we demonstrate DNA-PAINT imaging with approximately 5 nm resolution using a 4nucleotide hybridization domain that is 43% shorter than previously reported probes. Imager probes with such short hybridization domains are key for improving detection on DNA nanostructure devices because they have the capability to target a larger number of binding domains per localization unit. This is essential for metrology applications such as Nucleic Acid Memory (NAM) where the information density is dependent on the binding site length. The selected imager probes reported here present imaging resolution equivalent to current state-of-the-art DNA-PAINT probes, creating a strategy to image shorter DNA domains for nanoscience and nanotechnology alike.

KEYWORDS: DNA-PAINT, imager probe, BNA, binding domain, super resolution microscopy, TIRF

NA-PAINT is a variation of Points Accumulation for Imaging in Nanoscale Topography (PAINT)¹ superresolution microscopy (SRM), in which transient hybridizations between dye-labeled DNA oligonucleotides (imager probes) and complementary target strands (docking strands) are used to achieve spatial resolution below the diffraction limit of light.² Since its inception in 2010,³ this technique has achieved sub 5 nm resolution^{4,5} by optimizing

Received: May 23, 2024 Revised: July 19, 2024 Accepted: July 24, 2024 Published: August 7, 2024





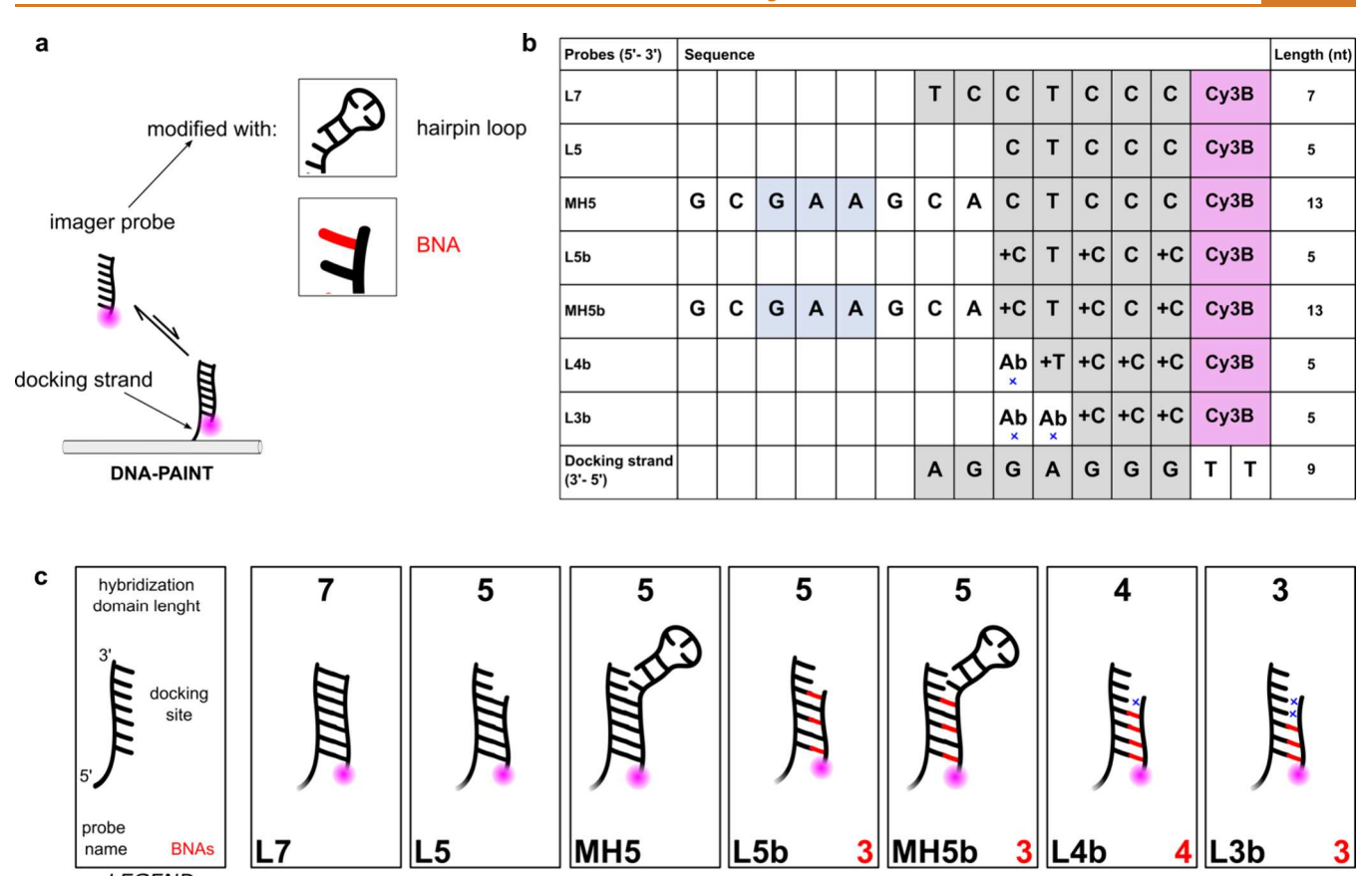


Figure 1. Modified short-domain probes. The two modifications (hairpin loop or BNA) used to generate imager probes with short hybridization domains are illustrated in (a). All the probes' sequences used in this study, together with their complementary strands, are listed in (b) and their structure graphically represented in (c). (b) Hybridization domains are highlighted in gray and loop regions in blue. BNA modified nucleotides are denoted with "+" sign while "Ab" and a blue cross indicate a nonbinding abasic site.

imager probe sequence design and buffer conditions. More recently, Ångstrom-level resolution was achieved by sequential imaging of multiple localizations of a single target.

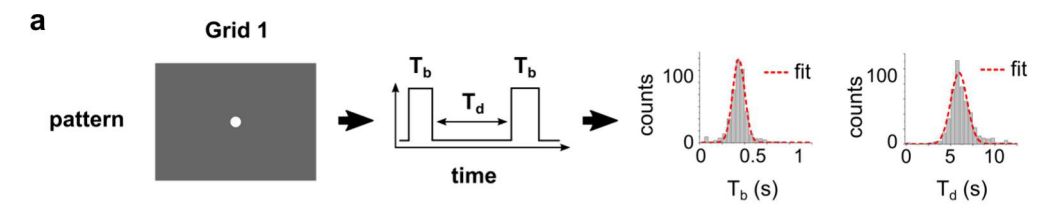
However, the complex and dynamic environment makes such resolutions very difficult to achieve in cells. Therefore, state-of-the-art DNA-PAINT achievements are first validated in more controllable *in vitro* environments such as DNA origami templates. The use of these artificial DNA nanostructures is key to benchmark different imager probes design adaptations and to test their highest performance before any successive evaluations. This has inevitably supported DNA-PAINT to naturally grow into a metrology technique for *in vitro* applications possibly distant from biological settings. In these studies, the imager probe sequence design, the buffer conditions, and the DNA origami docking platform have been constantly optimized for a specific engineered solution. 5,7–9

Historically, imager probes were designed by tuning their bound (bright time, $\tau_{\rm b}$) and unbound (dark time, $\tau_{\rm d}$) states to maximize photon flux, signal-to-noise ratio, and single-emitter events; resulting in probes 7 to 35 nucleotides (nt) long. 4,14 While elusive, imager probes shorter than 7 nt are vital for *in vitro* applications such as digital Nucleic Acid Memory (dNAM)¹¹ that require high resolution and short target specificity. Balancing both, supports reading dense information arrays made from DNA in x, y, and potentially in z. 8,9 Engineering probes below 7 nt is difficult because DNA-duplex stability, and thus $\tau_{\rm b}$, decreases exponentially as the hybridization domain length decreases. This results in imager probes with submilli-

second binding times, and hence an insufficient number of photons per blinking event to be recorded via state-of-the-art cameras and chromophores. 2,9

In this study, we compare the performance of a state-of-the-art imager probe in the literature to probes that are shorter than 7 nt, and yet were engineered to have adequate stability. This study aims of providing improved probes for nanoscale metrology applications and preliminary probe design for DNA-PAINT in vitro detection. This was accomplished by structurally and chemically modified probe oligonucleotides to stabilize the probe-docking duplex and to create high-resolution probes with shorter binding domains. Specifically, we achieved structural stability using a hairpin-loop inspired by the guanosine-n-adenosine trinucleotide loop 15,16 and chemical stability by adding site-specific Bridged Nucleic Acid (BNA) nucleotides (Locked Nucleic Acid analogue) to the probe. In addition to increasing probes' oligonucleotide stability like LNAs (Locked Nucleic Acid) do, BNA improves binding specificity and resistance to nuclease degradation¹⁷ (for details see Table S5).

Rather than explore the vast sequence space available for probes, we adopted the sequence of the shortest known probe in the literature (named "PS3") from Schickinger et al. ¹⁴ As the PS3 sequence is 7 nt long of linear DNA, hereafter we refer to it as our control "L7" (Linear7). We then rationally designed six sequence-matched variants with hybridization domains 3 nt to 5 nt long, containing either hairpin loops, BNA-modifications, or both. Herein hairpin loops are referred to with the prefix "MH"



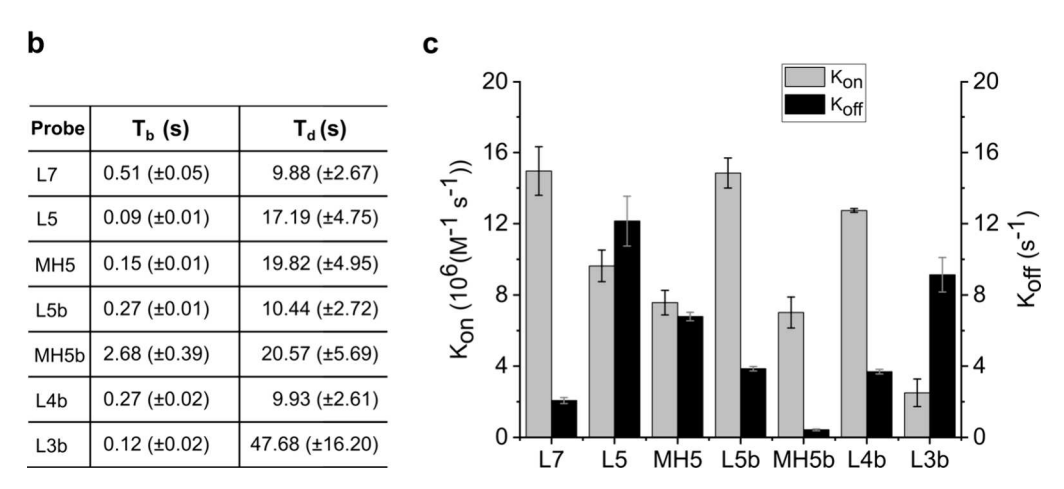


Figure 2. Short-domain probes kinetic properties. (a) Depicts the steps taken to acquire τ_b and τ_d . The values obtained are shown in (b) while calculated association and dissociation constants are in (c); uncertainties are standard errors of the mean values obtained from the Gaussian fit (see Methods).

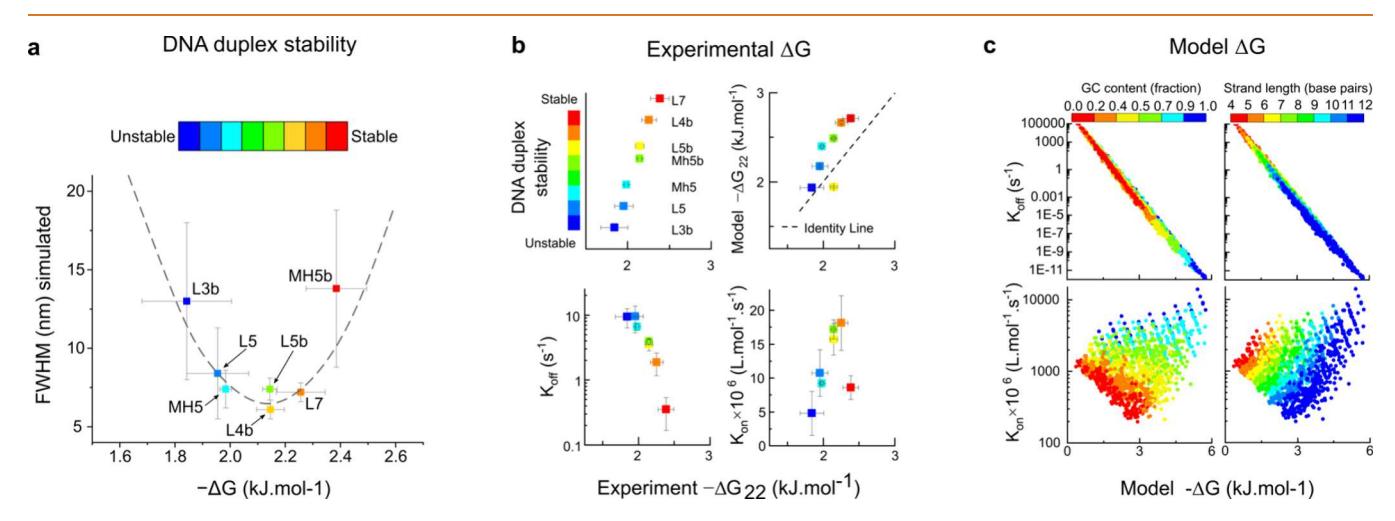


Figure 3. Experimental and model thermodynamic analysis. (a) ΔG values for each probe were calculated using $\tau_{\rm b}$ and $\tau_{\rm d}$ values (Figure 2) to rank probes by DNA-duplex stability (color coded) and plotted against their simulated resolution (FWHM) (see Methods). The dashed line (gray) serves to guide the eye to the U-shaped relationship observed between probe performance and ΔG , helping us identify the resolution minimum. (b) Top-left, experimental probe stability; top-right, predicted vs experimental probe stability, where the dotted line is the identity line, points to the left of the line indicate a model overestimate of the stability of the probe; bottom-left, experimental stability vs experimental $k_{\rm off}$; bottom-right, experimental stability vs experimental $k_{\rm off}$. (c) Theoretical nearest-neighbor kinetic rates from ref (18) and thermodynamic free energy of hybridization (19) as a function of nearest-neighbor ΔG_{22} for 1800 randomly generated strands, colored by fractional GC content (left) and strand length (right).

(Mini-Hairpin) and BNA with the suffix "b" (Figure 1). Using these modifications, we created imager probes possessing up to 43% shorter hybridization domains that achieve equivalent resolution to L7 in DNA-PAINT. The shortest variants' (3 nt to 4 nt) hybridization domains were entirely composed of BNA-modified bases (Figure 1b-c). However, as current synthesis restrictions (see Methods) require probes to be at least 5 nt long,

we used abasic sites to extend the sequence length without increasing the length of its binding domain (Figure 1b-c).

RESULTS AND DISCUSSION

Kinetic properties of short-domain probes. The imager probe's bright and dark time (τ_b and τ_d) are representative of the transient binding equilibrium that defines DNA-PAINT

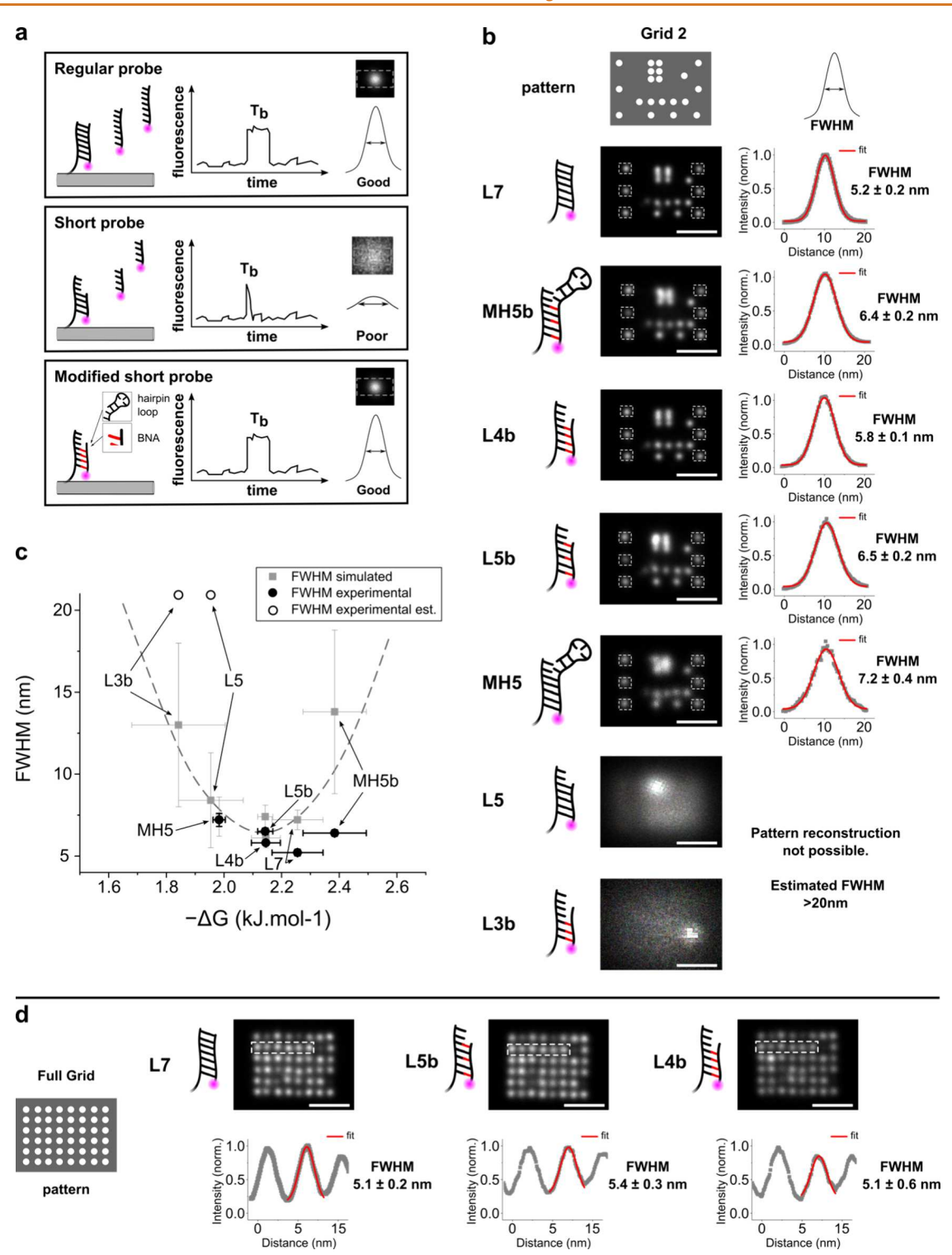


Figure 4. DNA-PAINT performance analysis of short-domain probes. (a) Illustration of how modifications to short-domain probes allow to reestablish high resolution. The resolution analysis using the Grid 2 pattern is shown in (b); a reconstructed image of the pattern is depicted on the left and an intensity profile across a single localization site is on the right. The plotted intensity is the mean of the pixel values indicated by the white dashed boxes in the image. The resolving power of the L5 and L3b probes was not sufficient to reconstruct the pattern images. Therefore, we estimated the FWHM of L5 and L3 to be greater than the average pattern gap: 20 nm. The experimental FWHM values (black circles) are plotted together with the simulation results from Figure 3a (gray squares) in (c). In this graph, hollow circles indicate the estimated FWHM values of the L5 and L3b probes, while the gray dashed line is the ΔG -based resolution prediction. (d) The best performing probes (L5b and L4b), together with the control L7, were analyzed using the Full Grid pattern (10 nm gap between sites). For clarity, the plotted profiles represent a section of the transects through the dashed white box in the image. The FWHM values are means analyzed from at least six localizations per experiment; uncertainties are single standard deviation from the mean. Gaps in the Full Grid likely arise from origami synthesis errors leading to unincorporated docking strands. Scale bars are 40 nm in width.

principle. The bright time (τ_b) is how long the imager probes bind to their docking strands. It also qualifies the number of photons collected per blinking event. In comparison, the dark time (τ_d) is the length of time between two binding events on the same localization. It influences the number of blinking events collected per unit time (Figure 2a). Longer bright times correspond to better achievable localization precision, while shorter dark times equate to faster image acquisition. A rule of thumb for DNA-PAINT is to ensure that the bright time is long enough to promote high precision and the dark time is as short as possible. 9,14

In order to analyze the short probe kinetics, we calculated $\tau_{\rm b}$ and τ_d values by monitoring hybridizations to a single docking strand protruding from an approximately 90 nm by 70 nm rectangular DNA-origami (Grid 1, Figure S1), as previously described (Figure 2a). For L7, we experimentally obtained a $\tau_{\rm b}$ of 0.51 \pm 0.05 s and $\tau_{\rm d}$ of 9.88 \pm 2.67 s. The $\tau_{\rm b}$ and $\tau_{\rm d}$ values obtained for modified probes ranged from 0.09 ± 0.01 s to 2.68 \pm 0.39 s and from 9.88 \pm 2.67 s to 47.68 \pm 16.20 s, respectively (Figure 2b). To further compare the kinetic properties of the probes we also calculated association (k_{on}) and dissociation (k_{off}) rates (Figure 2c). In particular, probes L5b and L4b have $k_{\rm on}$ and $k_{\rm off}$ values equivalent to L7, suggesting comparable binding stability despite their shorter hybridization domains. Intuitively, this is beneficial because these shorter probes produce a sufficient number of photons and a high localization precision in smaller footprint (Figure 4a). This is not, however, the case for all variants. For example, L5 and L3b do not demonstrate sufficient binding stability to yield a τ_b , and consequently k_{off} comparable to L7 (Figure 2b-c).

Simulated resolution and thermodynamics analysis. In order to better understand how the probe's kinetics affect DNA-PAINT imaging, we used the $k_{\rm on}$ and $au_{\rm b}$ values to simulate DNA-PAINT recordings (see Methods).² We then assessed each simulated probe's resolving power by measuring the Full Width at Half Maximum (FWHM) of a Gaussian curve fit to individual localizations. We also experimentally determined the Gibbs free energy (ΔG) of binding for each probe at 22 °C (see Methods) and plotted it against the simulated FWHM. Figure 3a indicates that probes with sharing similar k_{on} and k_{off} values are likely to demonstrate similar resolving power (see probes L5b and L4b). This does not seem to be the case if we consider probes with similar k_{off} but different k_{on} such as MH5 and L3b, which demonstrate quite different simulated resolutions (Figure 3a). This case points out the importance of k_{off} in predicting resolution performance, and led us to explore the possibility of predicting short probes' performance ab initio by using ΔG to model DNA-duplex stability and its effect on k_{off} (see Methods). We compared the experimentally determined ΔG of binding with the calculated ΔG model and correlated it with $k_{\rm on}$ and $k_{\rm off}$ parameters of randomly generated strands (Figure 3). The k_{off} and ΔG parameters were highly correlated in both experiments and model (Figure 3b-c). This supports the idea that any contribution (e.g., probe length, GC content, modified base, etc.) that increases stability will also reduce k_{off} proportionally (Figure 3 and Methods).

DNA-PAINT performance analysis of short-domain probes. In order to validate these kinetic and modeling results, we assessed the probes' ability to super-resolve two different patterns of docking strands (Grid 2 and Full Grid) extended from a DNA-origami platform (Figure 4b, d). We designed the Grid 2 pattern with the aim of testing the probes' ability to resolve a relatively sparse arrangement of docking strands

distributed at nominal distances of 4 to 40 nm (Figure S1). To quantify performance, we calculated the FWHM of probe localizations to a single point (see Methods). Similar to our simulation, the probes demonstrated a range of FWHM values of 5.2 ± 0.2 nm to 7.2 ± 0.4 nm when used in actual DNA-PAINT imaging (Figure 4b).

To evaluate the ability of our kinetics analysis to predict imaging resolution, we plotted the FWHM values for simulated and experimental results against ΔG (Figure 4c). Figure 4c shows that both simulated and experimental FWHM values follow a similar trend, with the lowest FWHM values observed between ΔG of 2.1 kJ mol⁻¹ and 2.3 kJ mol⁻¹. However, it is important to note that the three probes at the ends of the ΔG range performed substantially different from their simulation. For example, L5 and L3b showed worse resolution while MH5b showed better resolution than its simulated values (Figure 4c). At the low end of the ΔG range, the resolution obtained with L5 and L3b was insufficient to resolve individual docking strands, and accurately estimating FWHM values (Figure 4b). At the other end of the ΔG range, the experimental FWHM value of MH5b is considerably lower than the simulation predicted (Figure 4c). The source of this discrepancy can be the excessively long bright time of MH5b, which was 2.68 ± 0.39 s (Figure 2b). When incorporating this value into the Picasso-Simulate software package, a too low blinking rate resulted to provide good simulated accuracy within the low number of frames analyzed (see Methods). When compared to its counterpart probe without BNA (probe MH5), MH5b has a substantially lower k_{off} (Figure 2c). This indicates an increased stability of the hybridized state -confirmed by a lower ΔG - that presumably allows the probe to achieve a better resolution than predicted. Unfortunately, MH5b's strong duplex stability and consequently longer τ_d (Figure 2b) impose imaging speeds that are simply too low to acquire a viable DNA-PAINT image;^{2,5} reinforcing the importance of k_{off} when predicting DNA PAINT performance.

In the DNA-PAINT literature, imager probe sequence design, and buffer conditions have been refined to achieve performance gains in imaging speeds, lateral resolution, and multiplexing. ^{8–10} Although such performance gains are valuable, other more application-specific performance metrics are emerging. Depending on the application focus, certain DNA-PAINT qualities can be preferred over others. For example, in our NAM research where DNA-PAINT reads spatially encoded information in high-density arrays made from DNA origami, shorter binding domains provide a greater return on investment than incrementally improving the imaging speed and accuracy based on how rectilinear information scales in x, y, and z.

Albeit using a much shorter binding domain, the simulated and experimental lateral resolution of L5b and L4b, rival L7's (Figure 4b) representing a successful advancement. While these two probes achieve a resolution comparable to L7, they also have slightly shorter τ_b values and thus faster disassociation rates. We speculate that with a higher photon-rate (i.e., using a brighter chromophore label), these probes could deliver faster image acquisitions than Figure 4.9 To check this, we tested them within using a NAM substrate. The results reported in Figure S15 show how L5b and L4b can resolve a NAM pattern using half of the exposure time previously reported in the NAM study and acquiring 25% less frames while maintaining FWHM resolution values below 6 nm (Figure S15).

Considering their balanced imaging speed, resolution, and kinetic performance, we selected LSb and L4b as the best

shorter-domain probes candidates for further evaluation. In order to test their overall performance in a crowded DNA-PAINT environment, where crosstalk and nearest-neighbor effects are more likely to occur, 9,20 we imaged them on a Full Grid pattern in which 48 docking strands are located approximately 10 nm apart in a 6 by 8 matrix (Figure S1). Figure 4D indicates that L5b and L4b performed well in these conditions, achieving a localization resolution under 5.4 \pm 0.3 nm. This demonstrates a comparable resolution to L7, but with a 43% shorter hybridization domain length.

These results are particularly advantageous in applications where the detection of a shorter target sequence is key for improvement. While they do not show a better resolution than L7, L5b and L4b probes provide a path to detect shorter DNA sequences without compromising resolution, bringing along a good set of binding/unbinding rates able to match imaging performance only achieved with longer hybridization domain probes before (Figure 4a). We analyzed their multiplexing potential within the scope of NAM: two identical domains were stacked onto each other to test the probes' ability to detect multiple targets on the same docking strand. Figure S13 shows how L5b and L4b outperform L7 in double stacking recognition. In particular, as the binding domain shortens, the ability to access a double stack domain increases substantially (Figure \$13f). A more thorough analysis is needed to explore the full multiplexing potential of L5b and L4b, but based on this analysis it is clear that using shorter binding domain probes represents a step forward in multiple domain detection (Figure S13).

The use of the Full Grid pattern provides a better understanding of other aspects of the DNA-PAINT imaging besides pure resolution. In such a crowded environment the transient binding reactions can be hindered by cross talk and steric hindrance. In particular, we were concerned on crosshybridization of one probe over multiple dockings strands and/ or multiple probes over the same docking strand. While the analysis on Full Grid did not raise these concerns, showing good averaged localizations (Figure 4d), its 10 nm spacing may not be dense enough to enhance the above-mentioned issues. Hence, we preliminarily analyzed the selected probes on a section of docking strands pattern with an approximately 4 nm spacing. Figure S14 shows how L5b and L4b are able to differentiate localization sites that are 4 nm apart with resolution comparable to or better than L7. While an analysis on a wider range of targets is needed to rule out the variety of possible cross-talk reactions, Figure S14 clearly shows how shorter binding domain probes can work in tight spacing without additional cross-talk or steric hindrance when compared to longer probes. It is fair to expect that shortening the domain sequence will result in less specificity and so higher probability of cross-talk. That is why this preliminary result is encouraging, especially within the NAM application where being able to detect points in tighter space will enable greater information density and device scalability.¹¹

CONCLUSIONS

Using structural and chemical modifications of imager probes, we describe an approach for high-resolution DNA-PAINT imaging using shorter hybridization domains. The structural changes involved hairpin loops, the chemical changes used BNA modifications, and a hybrid approach combined both. BNA modifications were the most successful, resulting in an imager probe with a hybridization domain of 4 nt demonstrating approximately 5 nm resolution. This domain length is 3 nt shorter than the shortest reported in literature. ¹⁴ Moreover, the

binding efficiency of the top probes is comparable to the control L7 and it is not affected by different pattern density as shown by quantitative analysis on the Grid 2 and Full Grid patterns (Figure S12). On the contrary, L5b and L4b present slightly better binding efficiency than the control L7 when applied to a denser pattern (Figure S12). This result, together with the 4 nm spacing analysis (Figure S14), supports the ability of these shorter domain probes to work well in crowded and dense arrays, suggesting that their lower steric hindrance could be advantageous in tight spaces and crowded environments.

To increase the predictive capacity of probe performance, we also report a method for modeling thermodynamic properties. Modeling a probe's Gibbs free energy makes it possible to screen probe sequences before imaging and can guide the rational design of imager probes. Using tools such as this, we expect further probe optimization to drive performance gains.

Finally, probes with short hybridization domains provide a route for improving DNA-PAINT imaging in nanoscale metrology applications such as NAM¹¹ or DNA origami data cryptography. 12 For example, shorter hybridization domains may expand the capability to detect larger number of binding sites per localization unit. Our preliminary analysis indicates that using shorter binding domain probes represents a sincere advantage on multiple domains detection with respect to L7: an encouraging starting point for additional multiplexing. This is essential for applications such as NAM where the information density is dependent on the binding domain length. 11 Moreover, imaging analysis on 4 nm spacing pattern clearly shows how the reported shorter binding domain probes do not present additional cross-talk or steric hindrance challenges than those of longer probes (Figure S14). Collectively, these features are of importance for DNA-PAINT applications where tight space and controlled environment allow to push the limit toward shorter DNA sequence targets. 11–13 Although this study does not report performance analysis of DNA-PAINT on biological samples, as this falls out of its scope, the results serve as a starting point for future validation of DNA-PAINT shorter probes in biological environments.

METHODS

Buffers. All materials and reagents used in this study are outlined in Table S1. Three buffers were used in this study: deposition, imaging and AFM. The deposition buffer contained 0.5× Tris-borate-EDTA (TBE) and 18 mmol L-1 MgCl2 and is used to deposit the DNA origami structures onto the glass coverslip prior super resolution imaging. The imaging buffer contained 0.5× TBE and 75 mmol L-1 MgCl2 with the supplement of 200 nmol L-1 Protocatechuate 3,4-dioxygenase pseudomonas, 1 mmol L-1 Trolox and 5 mmol L-1 PCA (added prior to imaging) as oxygen scavenger solution. The 3,4 (dihydroxybenzoic) Protocatechuic acid was added to the imaging buffer immediately before the start of a DNA-PAINT acquisition. The AFM buffer contained 0.5× Tris-Acetate-EDTA (TAE) and 12 mmol L-1 MgCl2 and was used to dilute the DNA origami solution on the MICA support before Atomic Force Microscopy imaging.

Imager Probes. The Cy3B-labeled DNA short oligonucleotides used as imager probes in this study were obtained from Bio-Synthesis Inc. (Lewisville TX, USA) with dual-HPLC purification and BNA modifications as highlighted in Figure 1B. As Bio-Synthesis Inc. sets a 5 nt minimum length for any DNA oligonucleotide synthesis, we ordered abasic sites to decrease the length of the hybridization site in some of the imager probes (see Figure 1b). To guarantee good availability and minimize steric hindrance between imager probe and docking strands, for mini-hairpin loops, we introduced an additional unpaired base before the loop's stem and we limited BNA modifications to 3 nt of the 5 nt making up the hybridization site. However, for smaller sites with no

mini-hairpins loops (<5 nt), all nucleotides were BNA modified (see Figure 1b). For completeness, we calculated the signal-to-noise ratio of each probe in the recordings and we calculated the specificity of the shorter PS3 sequence binding against a non-complementary docking strand (Figure S11).

DNA Origami Platforms. Rectangular 2D DNA origami (dNAM) structures (approximately 90 nm by 70 nm) were designed based on previous work by Rafat et al. 21 with 48 potential docking strand sites arranged in a 6 by 8 matrix as previously described. 11 Using the protocol described by Schnitzbauer et al. 2 a mixture of normal staple strands and unmodified extended staple strands (Table S2) were selected to fold the M13 scaffold into the designed shape, with extended strands located at positions described in the design patterns. Three different patterns of extended staples were used in this study: single extended site ("Grid 1"), different distances extended strands pattern ("Grid 2") and full extended strands matrix ("Full Grid"). A detailed list of staples and representations of the three matrices is shown in Table S2 and Figure S1

We assembled individual origami designs by combining 22 nmol L-1 M13mp18 with 10× unmodified stands, 50× extended strands, 0.5× TAE and 18 mmol L-1 MgCl2 (in nuclease-free water; 80 μL total volume) and folding in a Mastercycler nexus thermal cycler (Eppendorf, Hamburg DE) using the following heating cycle: [1 min 90 °C, 2 min 80 °C, then from 80 to 20 °C over 12 h]. We purified the origami by running them on a 1% agarose gel containing 0.5× TBE and 8 mmol L-1 MgCl2, excising the single sharp band, and collecting the exudate of the crushed gel piece. Sharp triangle origami used as fiducial markers were prepared similarly, as previously described 11 (see table S3 for oligonucleotide sequences). All purified origami were stored in the dark at 4 °C until use.

Sample Preparation. The formed DNA origami structures were deposited on glass substrates using a microfluidic cell (sticky-Slide, Ibidi GmbH) equipped with inlet and outlet tubes to allow buffer exchange and washing steps between different imager probes solutions. Borosilicate glass slides (25 mm by 75 mm, #1 Gold Seal Coverglass) were sonicated in a volume fraction of 0.1% Liquinox and nanopure water (1 min in each) to remove contaminants and dried at 40 °C for at least 30 min. The coverslips were then, rinsed with methanol and nanopure water and stored at 40 °C prior to use. The glow discharge technique previously described by Green et al.²² was used to deposit DNA origami onto glass coverslips using a PELCO easiGlow Glow Discharge Cleaning System (Ted Pella Inc.). Briefly, coverslips that had been cleaned were exposed to glow discharge generated using 20 mAmp at 0.5 mbar for 75 s. For DNA-PAINT analysis, the sticky-Slide flow cell (approximately 50 μ L channel volume) was glued to the coverslip and the DNA origami solution deposited by introducing 600 μ L of 0.02 nmol L-1 DNA origami (a mixture of dNAM origami, and sharp triangle origami added as additional fiducial markers, in deposition buffer) into the channel and incubated for 30 min at room temperature. After deposition, the flow chamber was rinsed with 3 mL of deposition buffer (with no DNA origami) and mounted on the Fluorescence Microscope.

Super Resolution Microscopy. Immediately before imaging, the imager probe solution (imager probe strand in imaging buffer) was supplemented with 5 mmol L-1 PCA to initiate the oxygen scavenger reaction. DNA origami were imaged below the diffraction-limit of light via DNA-PAINT using an inverted Nikon Eclipse Ti2 microscope from Nikon Instruments in Total Internal Reflection Fluorescence (TIRF) mode. The images were acquired using an integrated Perfect Focus System from Nikon Instruments; an oil-immersion CFI Apochromat 100x TIRF objective, with a 1.49 numerical aperture, plus an extra 1.5× magnification from Nikon Instruments; and a 405/488/561/647 nm Laser Quad Band Set TIRF filter cube from Chroma. A 561 nm laser source excited fluorescence from the DNA-PAINT imager strands within an evanescent field extending a few hundred nanometers above the surface of the glass coverslip. The emitted fluorescence was imaged onto the full chip with 512 by 512 pixels (1 pixel = approximately 107 nm) using a ProEM EMCCD camera from Princeton Instruments at selected exposure time (150 ms). Images with blinking events were recorded into a stack (typically 40 000 frames per recording) using Nikon NIS-Elements version 5.20.00 from Nikon Instruments prior to processing and analysis.²²

Binding Rates Analysis. Immediately before imaging, the imager probe solution (imager probe strand in imaging buffer) was supplemented of 5 mmol L-1 PCA to initiate the oxygen scavenger reaction. This time, the single docking strand pattern was used (Grid 1) in order to ensure the blinking events were recorded only from one strand localization and not overlapping neighbors' effect. The blinking events were acquired with a 50 ms exposure time and 10000 frames were collected each acquisition. τ_b and τ_d were calculated using Picasso-Render software package to gather all the picked locations properties and collecting all the data with a custom-written code. Then the data were analyzed in OriginPro Version 2019b (OriginLab) to generate time distribution graphs for each probe at 3 nmol L-1, 10 nmol L-1, 20 nmol L-1, and 50 nmol L-1 concentrations. The distributions were then fitted by Gaussian distribution to calculate the mean time (see Figures S2 to S8). The uncertainties reported are standard uncertainties of the mean value. Using $\tau_{\rm b}$ and $\tau_{\rm d}$ values, the association and dissociation constants were also calculated in function of concentration (see Figures S2 to S8). The mean and standard uncertainties of all τ_b , τ_d values and $k_{\rm on}$, $k_{\rm off}$ values are reported in Figure 2b and c.

Data Analysis. After recording a DNA-PAINT images stack, the center position of signals (localizations) emitted by imager probes, transiently binding to DNA origami docking strands, were identified using the ImageJ ThunderSTORM plugin.²³ The localizations were rendered and then drift-corrected using the Picasso-Render software package, as described by Schnitzbauer et al.² When needed, the rendered origami patterns were picked and averaged together using Picasso-Average software package. Data visualization and peak fitting of image data for PSF analysis were performed using OriginPro Version 2019b (OriginLab).²²

Data Simulation. A localizations pattern with a 10 nm spacing was created using Picasso-Design software package. This was then imported in the Picasso-Simulate software package and 1000 frames of acquisitions were simulated based on the $k_{\rm on}$ and $\tau_{\rm b}$ input values of each probe at 3 nmol L-1 concentration. In each simulated acquisition 700 structures were generated with 100% localization sites incorporation, PSF was set at 1 pixel and background level at 10. Camera parameters were updated accordingly to the imaging parameters used for the Figure 2 analysis (see Super Resolution Microscopy section). To note that Picasso-Simulate software package does not use $k_{\rm off}$ value as input in its simulations. The simulated images were generated and single localization spots have been analyzed by collecting their intensity profile and calculating the fwhm of the Gaussian fit. The uncertainties were calculated identically to that of experimental data: one standard deviation from the mean value.

Imager Probes Thermodynamics Analysis. Experimental quantification of Gibbs free energy of probe binding at the laboratory temperature, (22.10 ± 0.56) °C, ΔG_{22} (referred in the text as ΔG), as defined in eq 1 where C is the concentration, T is the temperature and R is the gas constant.

$$\Delta G_T = -\ln \left(\frac{K_{off}}{C^* K_{on}} \right) RT \tag{1}$$

These energies are shown in Figure 3B. Uncertainties on the experimental ΔG_{22} were assumed to be not correlated and due to both uncertainties in temperature, $k_{\rm on}$, and $k_{\rm off}$. Pipetting uncertainty in concentration was neglected. As analytical propagation of uncertainty through a logarithm is nontrivial, we assumed the rate related component was the variation in ΔG_{22} when calculated at \pm one standard deviation in $k_{\rm on}$ and $k_{\rm off}$. To make a generous assumption the (+) standard deviation for $k_{\rm on}$ was matched to the (–) standard deviation for $k_{\rm off}$ and vice versa, to ensure that the reported uncertainties overreported, rather than underreported, compared to reality. This was combined in quadrature with the temperature contribution.

We then compared our experimental probe energetics to a thermodynamic nearest neighbor model. Predicting the nearest neighbor ΔG_{22} for the probes required a number of assumptions.

These include that the contribution of the Cy3B dye is identical to the Cy3 dye for which there is a correction; ²⁴ and that the contributions of BNA are identical to LNA, ²⁵ which is reasonable given their similar mechanism of stabilization; the contribution of dangling ends; ²⁶ and that abasic sites do not contribute meaningfully to hybridization stability. Figure S10 gives a visual description of these correction factors

It should be noted that the MHS and MHSb predictions require multiple contributions that we could not easily model, specifically a single position that is simultaneously a mismatch with a dangling end, and which would benefit from base stacking due to the neighboring hairpin. In this case we chose to estimate the energetics as that of two dangling ends.

Figure 3b shows the experimental and predicted ΔG_{22} for each of the probes. The dotted line is the identity line, any data point to the right of it indicates model overestimation, while any point on the left indicates model underestimation. Figure 3b shows good agreement between the model and experiments, particularly given the complexity of the probes and number of assumptions required. This indicates that preliminary thermodynamic modeling may support probe design.

Imager Probes Kinetics Analysis. As a kinetic nearest neighbor model for DNA hybridization has been recently published, 18 it does not yet have the correction factors necessary to properly model our probes. However, it is useful to examine the anticipated effect of probe sequence and length, and to compare to our experimental $k_{\rm on}$ and $k_{\rm off}$. We compared the kinetic model for DNA hybridization to the thermodynamic model for 1800 randomly generated sequences of length 4 nt to 12 nt, as well as to our experimental data. We also compared the results for these sequences when using the parameter set for 1 mol·L-1 NaCl buffer and for 2 mmol L-1 buffer. The data is not shown for the 2 mmol L-1 buffer solution. Figure 3c shows the predicted $k_{\rm on}$ and $k_{\rm off}$, in 1 mol·L-1 NaCl buffer plotted against the nearest neighbor predicted ΔG_{22} . The data is replotted twice to show color maps for strand GC content and strand length as in Figure 3a. These figures indicate that the $k_{\rm off}$ does not appear much perturbed by surface binding, difference in salt concentration, or additional energetic contributions. In contrast, experimental k_{on} values differ considerably from the predicted values. This is unsurprising as the experimental salt concentration (75 mmol L-1) is much higher than in the model. In addition, steric hindrance should substantially change k_{on} .

This kinetics analysis indicates that any source of stability, ΔG_{22} , for a probe may cause a predictable change in $k_{\rm off}$. Additionally, Figure 3c indicates that $k_{\rm on}$ is dependent on GC content, but not reliably on ΔG_{22} . Based on this kinetic model, increasing strand fractional GC content will likely improve $k_{\rm on}$.

Atomic Force Microscopy. AFM analysis was conducted on freshly cut mica. 4 μ L of a dNAM origami sample was deposited onto the substrate for 1 min and then 100 μ L of AFM buffer added to form a droplet on top of the sample. AFM imaging was performed with a Dimension-FastScan system from Bruker (Billerica MA, USA) set to amplitude modulation mode. Imaging was carried out in liquid with a set-point ratio between the free amplitude and imaging amplitude of approximately 0.7. The FastScan D cantilever was supplied by Bruker, with a nominal spring constant of 0.25 N.m-1. Subnanometer amplitude was used to image DNA docking strand positions on every origami structure following the method of Tilt correction (line or plane flattening) was performed using WSxM²⁸ software package version 5.0 Develop 9.22 (Nanotec Electronica, Madrid, Spain) and a low-pass filter applied to remove noise (see Figure S9).

DNA-PAINT Imaging Resolution Analysis. The DNA-PAINT imaging resolution of the different probes was analyzed using the DNA origami platform "Grid 2" and "Full Grid" (see Figure S1). Each probe was imaged at 1 nmol L-1 concentration and keeping all the SRM acquisition parameters constant: 150 ms exposure time, 40 000 frames acquired and at approximately 130 μ W of laser power (laser flux: 0.012 uW/um2). After correcting the drift in the postprocessing, around 1000 super-resolved structures have been averaged together to generate an image for each probe (Figure 4b and d). The single localization spots have been analyzed by collecting the intensity profile from the image

and calculating the FWHM of the Gaussian fit. The uncertainties are one standard deviation from the mean value.

Several precautions were employed to correctly compare the profiles. The averaged imaged generated by the Picasso-Average software package has been opened with Picasso-Render software package where the zoom size and the minimum density were set constant. In addition, this step was used to generate the scale bar and set the blur to "none". The maximum density was adjusted to avoid saturation of the pixels. In this way the averaged image could be opened with ImageJ software as a 32-bit black and white image; the scale bar was set constant and the image intensity normalized.

The same dockings localization pattern position was used to compare the intensity profiles. The white spots were cropped, their intensity normalized and their profiles data generated selecting a box across the spots. Using Origin Pro software, the intensity profile was generated, fitted using a Gaussian function and the FWHM calculated for each probe. In the case of L5 and L3b probes the DNA-PAINT imaging quality was not sufficient to super resolve the pattern, consequently, the resolution analysis of the profiles was not possible (Figure 4b).

ASSOCIATED CONTENT

Supporting Information

The Supporting Information is available free of charge at https://pubs.acs.org/doi/10.1021/acsnano.4c06886.

DNA origami sequences, detailed kinetic analysis, Atomic Force Microscopy characterization, probes' energy contributions, quantitative and multiplexing analysis, additional resolution and high-speed acquisition analysis for selected probes, and nucleotide chemical modifications' structure analysis (PDF)

AUTHOR INFORMATION

Corresponding Author

William L. Hughes — Micron School of Materials Science & Engineering, Boise State University, Boise, Idaho 83725, United States; Present Address: Faculty of Applied Science, School of Engineering, University of British Columbia, Kelowna, B.C., V1 V 1 V7, Canada; orcid.org/0000-0003-0102-3573; Email: will.hughes@ubc.ca

Authors

Luca Piantanida — Micron School of Materials Science & Engineering, Boise State University, Boise, Idaho 83725, United States; Present Address: Faculty of Applied Science, School of Engineering, University of British Columbia, Kelowna, B.C., V1 V 1 V7, Canada; orcid.org/0000-0001-7378-0413

George D. Dickinson – Micron School of Materials Science & Engineering, Boise State University, Boise, Idaho 83725, United States

Jacob M. Majikes – National Institute of Standards and Technology, Gaithersburg, Maryland 20878, United States William Clay – Micron School of Materials Science & Engineering, Boise State University, Boise, Idaho 83725, United States

J. Alexander Liddle – National Institute of Standards and Technology, Gaithersburg, Maryland 20878, United States

Tim Andersen – Department of Computer Science, Boise State University, Boise, Idaho 83725, United States

Eric J. Hayden — Micron School of Materials Science & Engineering, Boise State University, Boise, Idaho 83725, United States; Department of Biological Sciences, Boise State University, Boise, Idaho 83725, United States

Wan Kuang – Department of Electrical & Computer Engineering, Boise State University, Boise, Idaho 83725, United States

Complete contact information is available at: https://pubs.acs.org/10.1021/acsnano.4c06886

Author Contributions

L.P. and W.L.H. conceived and supervised the study. L.P. also performed experiments, interpreted the data, and wrote the manuscript. G.D.D. conceived the experiments and analyzed data. J.M.M. performed, modeled and interpreted thermodynamics analysis. W.C. developed instrumentation. W.K. interpreted the data. All authors contributed to the writing and review of the manuscript.

Funding

This work has been supported by the National Science Foundation (Awards #1807809 and #2227626), by the Higher Education Council (HERC-2016) and by the Idaho Global Entrepreneurial Mission (IGEM-2016).

Notes

The authors declare no competing financial interest.

ACKNOWLEDGMENTS

We sincerely thank E. Graugnard and C. Watson for valuable discussions. We also thank N. Hallstrom for technical assistance and J. Dardis for copy-editing the manuscript.

REFERENCES

- (1) Sharonov, A.; Hochstrasser, R. M. Wide-Field Subdiffraction Imaging by Accumulated Binding of Diffusing Probes. *Proc. Natl. Acad. Sci. U. S. A.* **2006**, *103* (50), 18911–18916.
- (2) Schnitzbauer, J.; Strauss, M. T.; Schlichthaerle, T.; Schueder, F.; Jungmann, R. Super-Resolution Microscopy with DNA-PAINT. *Nat. Protoc* **2017**, *12* (6), 1198–1228.
- (3) Jungmann, R.; Steinhauer, C.; Scheible, M.; Kuzyk, A.; Tinnefeld, P.; Simmel, F. C. Single-Molecule Kinetics and Super-Resolution Microscopy by Fluorescence Imaging of Transient Binding on DNA Origami. *Nano Lett.* **2010**, *10* (11), 4756–4761.
- (4) van Wee, R.; Filius, M.; Joo, C. Completing the Canvas: Advances and Challenges for DNA-PAINT Super-Resolution Imaging. *Trends Biochem. Sci.* **2021**, *46* (11), 918–930.
- (5) Dai, M.; Jungmann, R.; Yin, P. Optical Imaging of Individual Biomolecules in Densely Packed Clusters. *Nat. Nanotechnol* **2016**, *11* (9), 798–807.
- (6) Reinhardt, S. C. M.; Masullo, L. A.; Baudrexel, I.; Steen, P. R.; Kowalewski, R.; Eklund, A. S.; Strauss, S.; Unterauer, E. M.; Schlichthaerle, T.; Strauss, M. T.; Klein, C.; Jungmann, R. Ångström-Resolution Fluorescence Microscopy. *Nature* 2023 617:7962 2023, 617 (7962), 711–716.
- (7) Filius, M.; Cui, T. J.; Ananth, A. N.; Docter, M. W.; Hegge, J. W.; Van Der Oost, J.; Joo, C. High-Speed Super-Resolution Imaging Using Protein-Assisted DNA-PAINT. *Nano Lett.* **2020**, *20* (4), 2264–2270.
- (8) Strauss, S.; Jungmann, R. Up to 100-Fold Speed-up and Multiplexing in Optimized DNA-PAINT. *Nature Methods* 2020 17:8 2020, 17 (8), 789-791.
- (9) Schueder, F.; Stein, J.; Stehr, F.; Auer, A.; Sperl, B.; Strauss, M. T.; Schwille, P.; Jungmann, R. An Order of Magnitude Faster DNA-PAINT Imaging by Optimized Sequence Design and Buffer Conditions. *Nature Methods* 2019 16:11 2019, 16 (11), 1101–1104.
- (10) Chung, K. K. H.; Zhang, Z.; Kidd, P.; Zhang, Y.; Williams, N. D.; Rollins, B.; Yang, Y.; Lin, C.; Baddeley, D.; Bewersdorf, J. Fluorogenic DNA-PAINT for Faster, Low-Background Super-Resolution Imaging. *Nature Methods* 2022 19:5 **2022**, 19 (5), 554–559.
- (11) Dickinson, G. D.; Mortuza, G. M.; Clay, W.; Piantanida, L.; Green, C. M.; Watson, C.; Hayden, E. J.; Andersen, T.; Kuang, W.;

- Graugnard, E.; Zadegan, R.; Hughes, W. L. An Alternative Approach to Nucleic Acid Memory. *Nat. Commun.* **2021**, *12* (1), 2371.
- (12) Rømer Thomsen, K.; Vallentin-Holbech, L.; Xylander, S.øv.; Wellnitz, K. B.; Tolstrup, J.; Nielsen, A. Søg.; Ewing, S. W. F. High-Speed 3D DNA-PAINT and Unsupervised Clustering for Unlocking 3D DNA Origami Cryptography. bioRxiv 2023, 23, 555281.
- (13) Kim, S. H.; Li, I. T. S. Super-Resolution Tension PAINT Imaging with a Molecular Beacon. *Angew. Chem., Int. Ed.* **2023**, 62 (7), No. e202217028.
- (14) Schickinger, M.; Zacharias, M.; Dietz, H. Tethered Multi-fluorophore Motion Reveals Equilibrium Transition Kinetics of Single DNA Double Helices. *Proc. Natl. Acad. Sci. U. S. A.* **2018**, *115* (32), No. E7512-E7521.
- (15) Yoshizawa, S.; Kawai, G.; Watanabe, K.; Miura, K. I.; Hirao, I. GNA Trinucleotide Loop Sequences Producing Extraordinarily Stable DNA Minihairpins. *Biochemistry* **1997**, *36* (16), 4761–4767.
- (16) Hirao, I.; Kawai, G.; Yoshizawa, S.; Nishimura, Y.; Ishido, Y.; Watanabe, K.; Miura, K.-i. Most Compact Hairpin-Turn Structure Exerted by a Short DNA Fragment, d(GCGAAGC) in Solution: An Extraordinarily Stable Structure Resistant to Nucleases and Heat. *Nucleic Acids Res.* 1994, 22 (4), 576–582.
- (17) Abdur Rahman, S. M.; Seki, S.; Obika, S.; Yoshikawa, H.; Miyashita, K.; Imanishi, T. Design, Synthesis, and Properties of 2',4'-BNANC: A Bridged Nucleic Acid Analogue. *J. Am. Chem. Soc.* **2008**, 130 (14), 4886–4896.
- (18) Rejali, N. A.; Ye, F. D.; Zuiter, A. M.; Keller, C. C.; Wittwer, C. T. Nearest-Neighbour Transition-State Analysis for Nucleic Acid Kinetics. *Nucleic Acids Res.* **2021**, *49* (8), 4574–4585.
- (19) Zhang, J. X.; Fang, J. Z.; Duan, W.; Wu, L. R.; Zhang, A. W.; Dalchau, N.; Yordanov, B.; Petersen, R.; Phillips, A.; Zhang, D. Y. Predicting DNA Hybridization Kinetics from Sequence. *Nature Chemistry* 2017 10:1 2018, 10 (1), 91–98.
- (20) SantaLucia, J. A Unified View of Polymer, Dumbbell, and Oligonucleotide DNA Nearest-Neighbor Thermodynamics. *Proc. Natl. Acad. Sci. U. S. A.* **1998**, 95 (4), 1460–1465.
- (21) Aghebat Rafat, A.; Pirzer, T.; Scheible, M. B.; Kostina, A.; Simmel, F. C. Surface-Assisted Large-Scale Ordering of DNA Origami Tiles. *Angew. Chem., Int. Ed.* **2014**, *53* (29), 7665–7668.
- (22) Green, C. M.; Schutt, K.; Morris, N.; Zadegan, R. M.; Hughes, W. L.; Kuang, W.; Graugnard, E. Metrology of DNA Arrays by Super-Resolution Microscopy. *Nanoscale* **2017**, *9* (29), 10205–10211.
- (23) Ovesný, M.; Křížek, P.; Borkovec, J.; Švindrych, Z.; Hagen, G. M. ThunderSTORM: A Comprehensive ImageJ Plug-in for PALM and STORM Data Analysis and Super-Resolution Imaging. *Bioinformatics* **2014**, *30* (16), 2389–2390.
- (24) Moreira, B. G.; You, Y.; Owczarzy, R. Cy3 and Cy5 Dyes Attached to Oligonucleotide Terminus Stabilize DNA Duplexes: Predictive Thermodynamic Model. *Biophys Chem.* **2015**, *198*, 36–44.
- (25) Hughesman, C. B.; Turner, R. F. B.; Haynes, C. A. Role of the Heat Capacity Change in Understanding and Modeling Melting Thermodynamics of Complementary Duplexes Containing Standard and Nucleobase-Modified LNA. *Biochemistry* **2011**, *50* (23), 5354–5368.
- (26) Bommarito, S.; Peyret, N.; John, S. Thermodynamic Parameters for DNA Sequences with Dangling Ends. *Nucleic Acids Res.* **2000**, 28 (9), 1929–1934.
- (27) Miller, E. J.; Trewby, W.; Farokh Payam, A.; Piantanida, L.; Cafolla, C.; Voitchovsky, K. Sub-Nanometer Resolution Imaging with Amplitude-Modulation Atomic Force Microscopy in Liquid. *J. Vis. Exp* **2016**, *118* (1), DOI: 10.3791/549.
- (28) Horcas, I.; Fernández, R.; Gómez-Rodríguez, J. M.; Colchero, J.; Gómez-Herrero, J.; Baro, A. M. WSXM: A Software for Scanning Probe Microscopy and a Tool for Nanotechnology. *Rev. Sci. Instrum.* **2007**, 78 (1), 013705.